

Sensor and Simulation Notes

Note 221

November 1976

Impedance of a Two-Conical-Plate
Transmission Line

F.C. Yang

K.S.H. Lee

The Dikewood Corporation, Westwood Research Branch
Los Angeles, California 90024

CLEARED
FOR PUBLIC RELEASE

PL/PA 5/15/97

Abstract

A combination of the techniques of stereographic projection and conformal mapping reduces the problem of calculating the TEM field distribution and impedance of two conical plates to that of a simple geometry for which the solution is known. Extensive tables and curves are given of the impedance of two conical plates for various cone angles and plate widths.

PL 96-1007

~~PL 96-1007~~

CONTENTS

Section		Page
I	Introduction	5
II	Method of Stereographic Projection	7
III	Method of Conformal Mapping	13
IV	Small Cone Angles	28
	Acknowledgment	33
	References	34

ILLUSTRATIONS

Figure		Page
1	Top and side views of the ATLAS I simulator.	6
2	Rectangular and spherical coordinate systems of two conical plates.	8
3	Stereographic projection of two conical plates onto two plates of circular arc.	12
4	The entire z-plane (Figure 3) is conformally mapped onto the region between two strips in the z_1 -plane.	14
5	The shaded region of Figure 4 is conformally mapped onto the upper-half t-plane	15
6	The entire upper-half t-plane (Figure 5) is conformally mapped onto a rectangle in the W-plane.	18
7	A suggested conformal mapping in which the parameter m would reduce to that often used for two parallel plates.	22
8	Geometric impedance factor f_g of two conical plates versus l/b .	23
9	Geometric impedance factor f_g of two conical plates versus b/a .	24
10	Geometric impedance factor \bar{f}_g of two parallel plates and the small-cone angle correction coefficient δ_{cp} .	32

TABLES

Table		Page
I	Mapping of boundary points.	16
II	Mapping of boundary points.	19
III	Values of the parameter m .	25
IV	Values of the geometric impedance factor f_g .	26
V	Values of the characteristic impedance Z_c of two conical plates.	27
VI	Values of \bar{f}_g and δ_{cp} .	31

I. INTRODUCTION

The most common type of bounded wave simulators consists of two plates with two conical sections and one cylindrical section. The conical sections are used as wave launcher and terminator, whereas the cylindrical section serves as the working volume in which test objects are placed. One such simulator is schematically illustrated in Fig. 1, which shows the top and side views of the future ATLAS I simulator.

The present note is concerned with the calculation of impedance of two conical plates. The TEM field distribution will be reported in a separate note. In Section II the conical line is stereographically projected onto a cylindrical line of two circular arcs on two different circles. This cylindrical line is further reduced, by the method of conformal mapping in Section III, to a simple structure of which the impedance is known. Tables and curves of the impedance are given for a variety of cone angles and plate widths. When the conical angle is small the deviation of the conical-plate impedance from the parallel-plate impedance is worked out explicitly in Section IV. Miraculously the small-cone-angle impedance formula works quite well even for moderately large cone angles if the plates' separation-to-width ratio is not too small. The impedance deviation is plotted as well as tabulated as a function of this ratio.

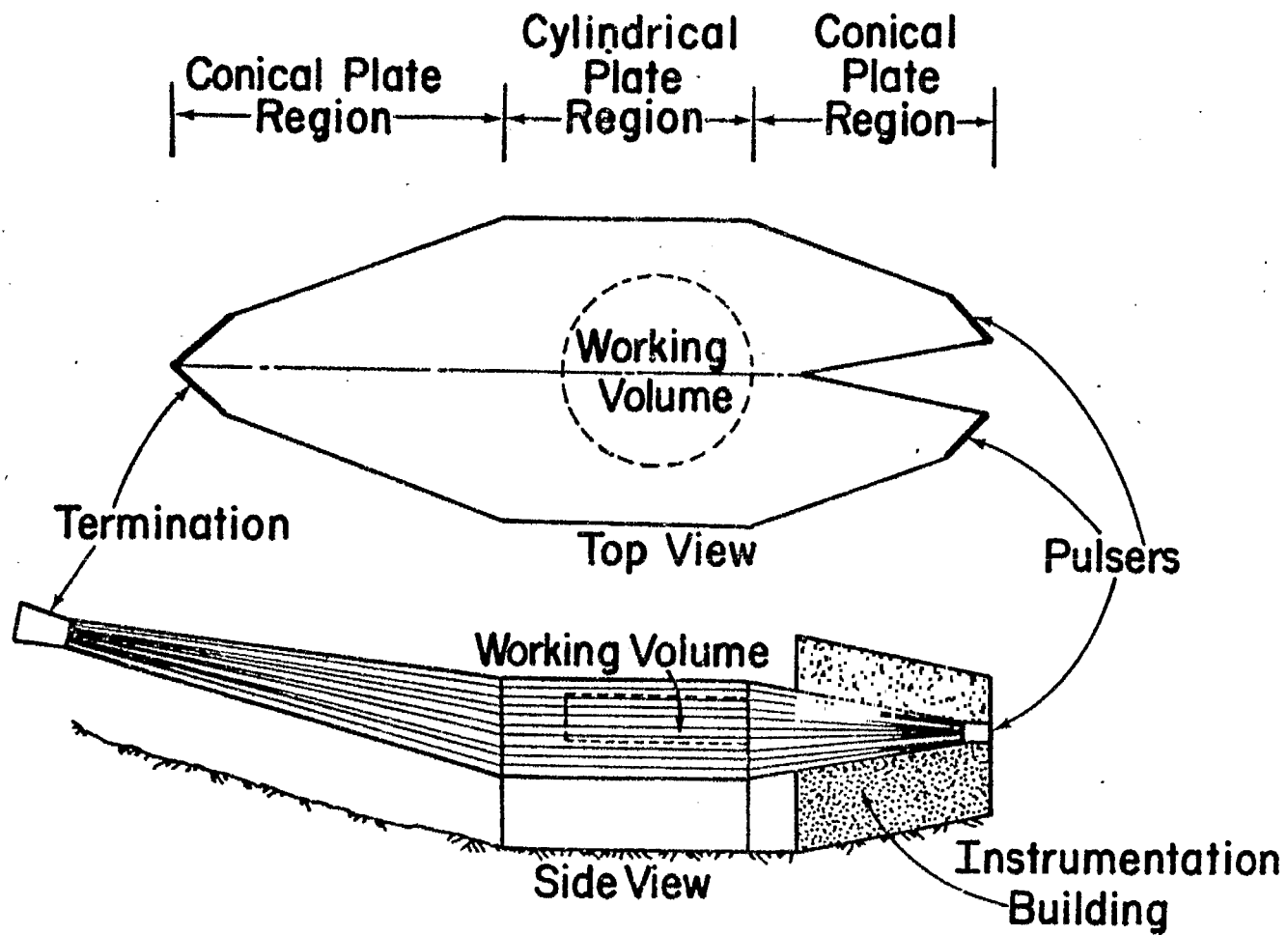


Figure 1. Top and side views of the ATLAS I simulator.

II. METHOD OF STEREOGRAPHIC PROJECTION

To analyze the TEM field distribution on two conical plates we employ the rectangular and spherical coordinate systems (x,y,z) and (r,θ,ϕ) as shown in Fig. 2. In the (x,y,z) coordinates the equations for the surfaces of the conical plates are given by

$$\begin{aligned}y &= \pm b(1 + z/\ell) \\|x/y| &\leq a/b \\z + \ell &\geq 0\end{aligned}\tag{1.a}$$

and, in the (r,θ,ϕ) coordinates by

$$\begin{aligned}\theta &= \pm\theta_0 \\ \pi/2 + \phi_0 &\geq \phi \geq \pi/2 - \phi_0\end{aligned}\tag{1.b}$$

where the "+" and "-" signs correspond, respectively, to the upper and lower plates. The angles θ_0 and ϕ_0 of the conical plates are determined by

$$\begin{aligned}\theta_0 &= \tan^{-1}(b/\ell) \\ \phi_0 &= \tan^{-1}(a/b)\end{aligned}\tag{1.c}$$

It is well known that the two conical plates as shown in Fig. 2 can support a spherical TEM wave propagating along the radial direction. The r -dependence of the complex potential W of a TEM wave can be factored out as [1]

$$W(r,\theta,\phi) = [U(\theta,\phi) + iV(\theta,\phi)]\exp(\pm ikr)/r\tag{2}$$

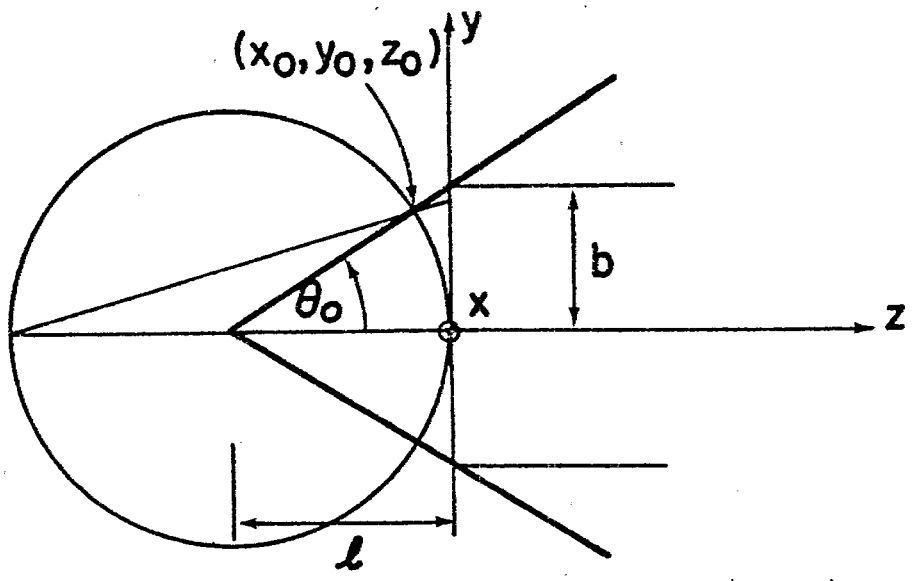
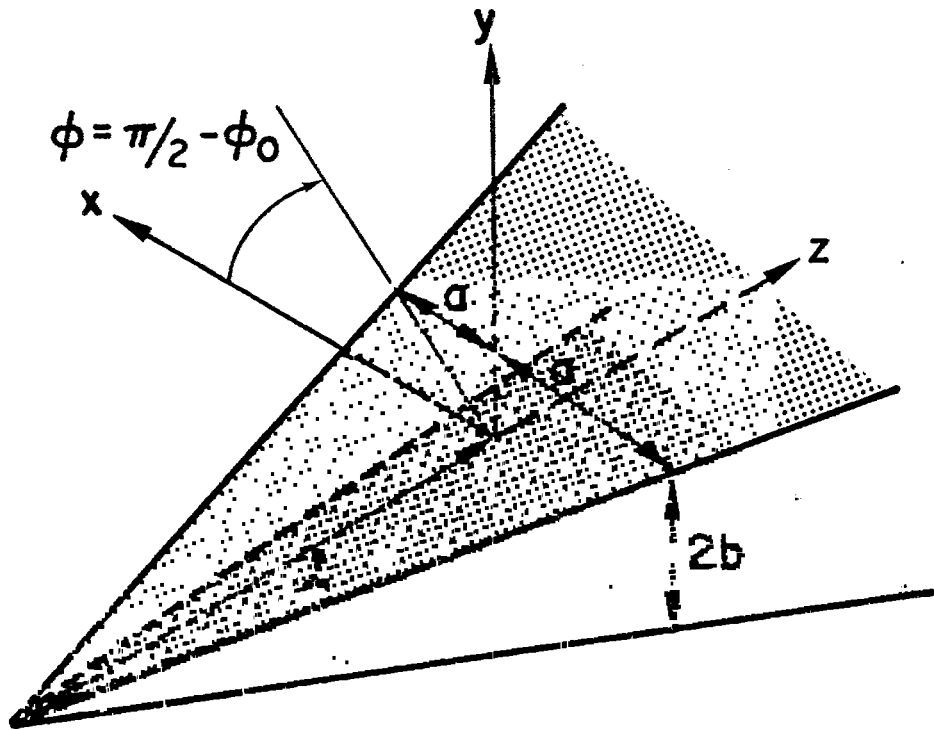


Figure 2. Rectangular and spherical coordinate systems of two conical plates.

where U and V satisfy the two-dimensional Laplace equation on a spherical surface

$$\sin \theta \frac{\partial}{\partial \theta} \left[\sin \theta \frac{\partial}{\partial \theta} \begin{pmatrix} U(\theta, \phi) \\ V(\theta, \phi) \end{pmatrix} \right] + \frac{\partial^2}{\partial \phi^2} \begin{pmatrix} U(\theta, \phi) \\ V(\theta, \phi) \end{pmatrix} = 0 \quad (3)$$

The functions U and V are uniquely determined once U (or V) is specified on the curves that are the intersections of the conical plates given by (1) and the spherical surface given by

$$r = \ell \quad \text{or} \quad x^2 + y^2 + (z + \ell)^2 = \ell^2 \quad (4)$$

The Laplace equation (3) on the unit sphere can be transformed to the ordinary two-dimensional Laplace equation in, say, the $z = 0$ plane by the method of stereographic projection through the following transformations [2]:

$$\begin{aligned} x &= 2\ell \tan(\theta/2) \cos \phi \\ y &= 2\ell \tan(\theta/2) \sin \phi \end{aligned} \quad (5)$$

by which (3) reduces to

$$\frac{\partial^2}{\partial x^2} \begin{pmatrix} U(x, y) \\ V(x, y) \end{pmatrix} + \frac{\partial^2}{\partial y^2} \begin{pmatrix} U(x, y) \\ V(x, y) \end{pmatrix} = 0 \quad (6)$$

The equation of the straight line connecting the point $(0, 0, -2\ell)$ and the point (x_0, y_0, z_0) is given by

$$\frac{x}{x_0} = \frac{y}{y_0} = \frac{z + 2\ell}{z_0 + 2\ell}$$

where the point (x_0, y_0, z_0) is shown in Fig. 2 and lies on the curves given by the intersections of the conical plates (1) and the spherical surface (4).

Hence, the intersections when projected onto the $z = 0$ plane satisfy the equations

$$\frac{x}{x_0} = \frac{y}{y_0} = \frac{2\ell}{z_0 + 2\ell} \quad (7.a)$$

which give

$$x = \frac{2x_0}{1 + (1 + z_0/\ell)} \quad (7.b)$$

$$y = \frac{2y_0}{1 + (1 + z_0/\ell)}$$

We are now in a position to find the equation that describes in the x, y -plane the curves that are the stereographic projections of the intersections between (1) and (4). To do this, we use (1.a), (4) and (7) to eliminate x_0 , y_0 and z_0 as follows:

$$\begin{aligned} x^2 + y^2 &= \frac{4(x_0^2 + y_0^2)}{[1 + (1 + z_0/\ell)]^2} \\ &= \frac{4\ell^2[1 - (1 + z_0/\ell)^2]}{[1 + (1 + z_0/\ell)]^2} \\ &= 4\ell^2 \left[1 - \frac{2(1 + z_0/\ell)}{1 + (1 + z_0/\ell)} \right] \\ &= 4\ell^2 \left[1 \mp \frac{2y_0/b}{1 + (1 + z_0/\ell)} \right] \\ &= 4\ell^2(1 \mp y/b) \end{aligned} \quad (8.a)$$

with

$$|x| \leq \frac{2\ell a}{\ell + \sqrt{\ell^2 + b^2 + a^2}} \quad (8.b)$$

The curves governed by (8) are shown in Fig. 3:

The potential function $V(x,y)$ and the stream function $U(x,y)$ on the projected $z = 0$ plane will be determined by specifying the value V on the two circular arcs given by (8). The characteristic impedance of the original two conical plates (Fig. 2) can be obtained from that of the two curved cylindrical plates (Fig. 3), since the two characteristic impedances are identical. The latter will be determined by conformal mapping in the next section.

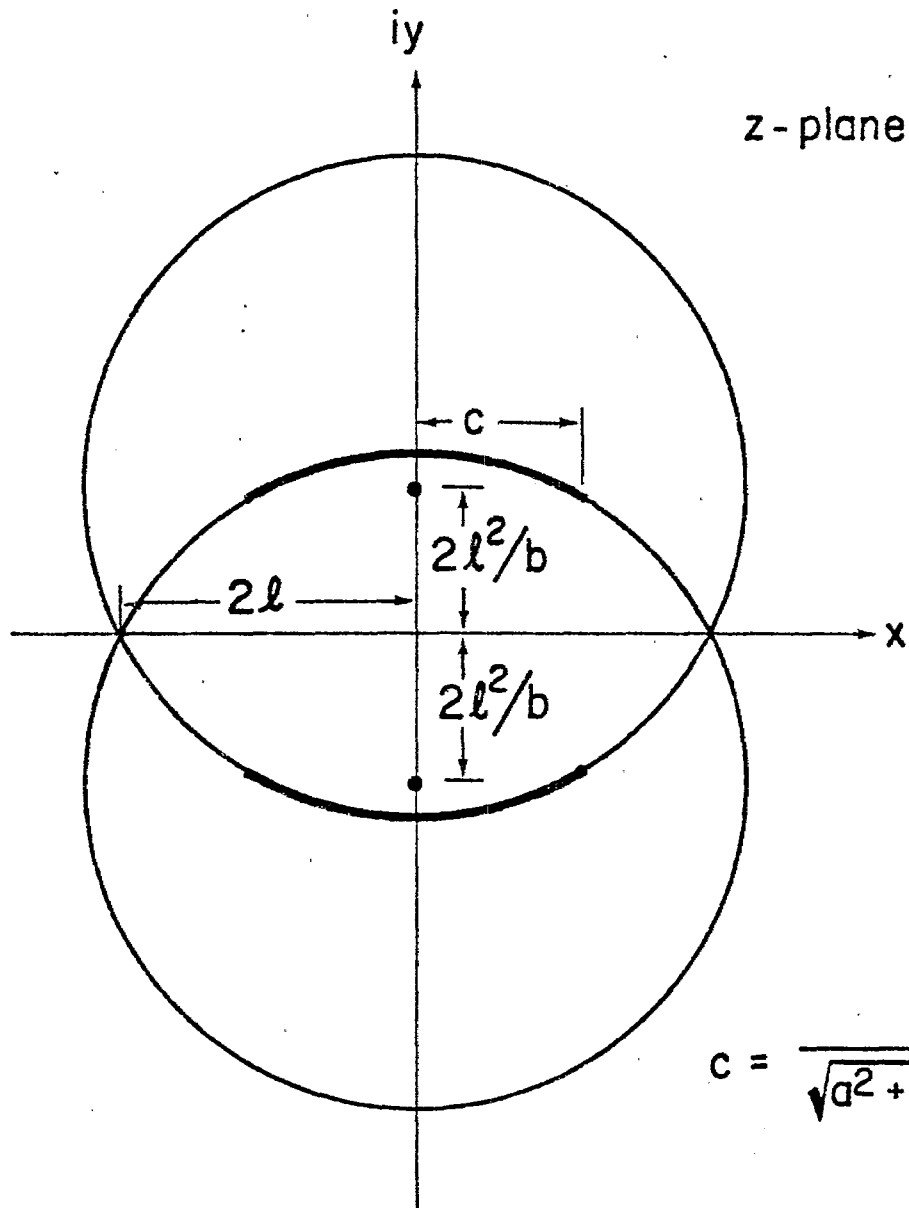


Figure 3. Stereographic projection of two conical plates onto two plates of circular arc.

III. METHOD OF CONFORMAL MAPPING

In this section we will determine the characteristic impedance of two curved cylindrical plates shown in Fig. 3. Successive conformal transformations will be applied to map the geometry of Fig. 3 into a rectangle (Fig. 6) from which the characteristic impedance is readily found.

First, we use the following hyperbolic transformation

$$z = 2l \tanh(z_1/2) \quad (9)$$

to map the whole complex z -plane into a region between two infinite parallel strips of separation 2π in the complex z_1 -plane as shown in Fig. 4. Here, $z = x + iy$ and $z_1 = x_1 + iy_1$. Under this transformation the two circular arcs are transformed into two parallel strips of width $2 \sinh^{-1}(a/b \sin \theta_0)$ and separation $2\theta_0$.

In the z_1 -plane we only need to consider the first quadrant because of the symmetry of the configuration. Using the following Schwarz-Christoffel transformation

$$z_1 = C_1 \int_0^t \frac{\sqrt{n} t' + (1-A_1)}{(1+\sqrt{n} t')\sqrt{(1-t'^2)(1-mt'^2)}} dt' + B_1$$

where $1 \geq m \geq n \geq 0$, $0 \leq |(1-A_1)/\sqrt{n}| \leq 1$, and A_1, B_1, C_1 are constants, one finds that the shaded quadrant of Fig. 4 is mapped into the upper half t -plane of Fig. 5. This integral can be carried out in terms of elliptic integrals and elliptic functions, namely,

$$z_1 = C_1 (u - A_1 [\Pi(n; u|m) - \sqrt{n} f(m, n, u)]) + B_1 \quad (10)$$

where $t = \sin \varphi = \operatorname{sn} u$, $m = \sin^2 \alpha$, and [3]

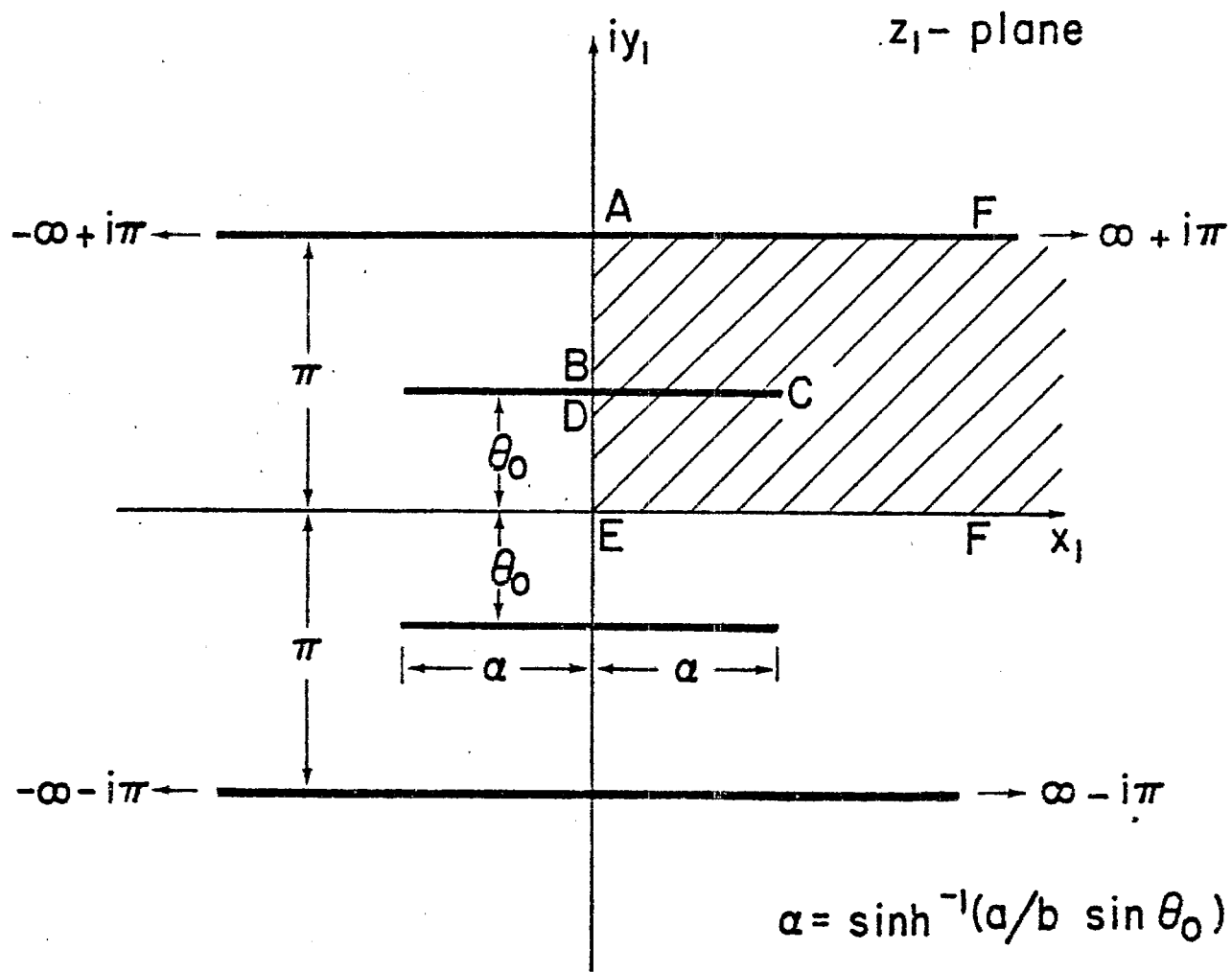


Figure 4. The entire z -plane (Figure 3) is conformally mapped onto the region between two strips in the z_1 -plane.

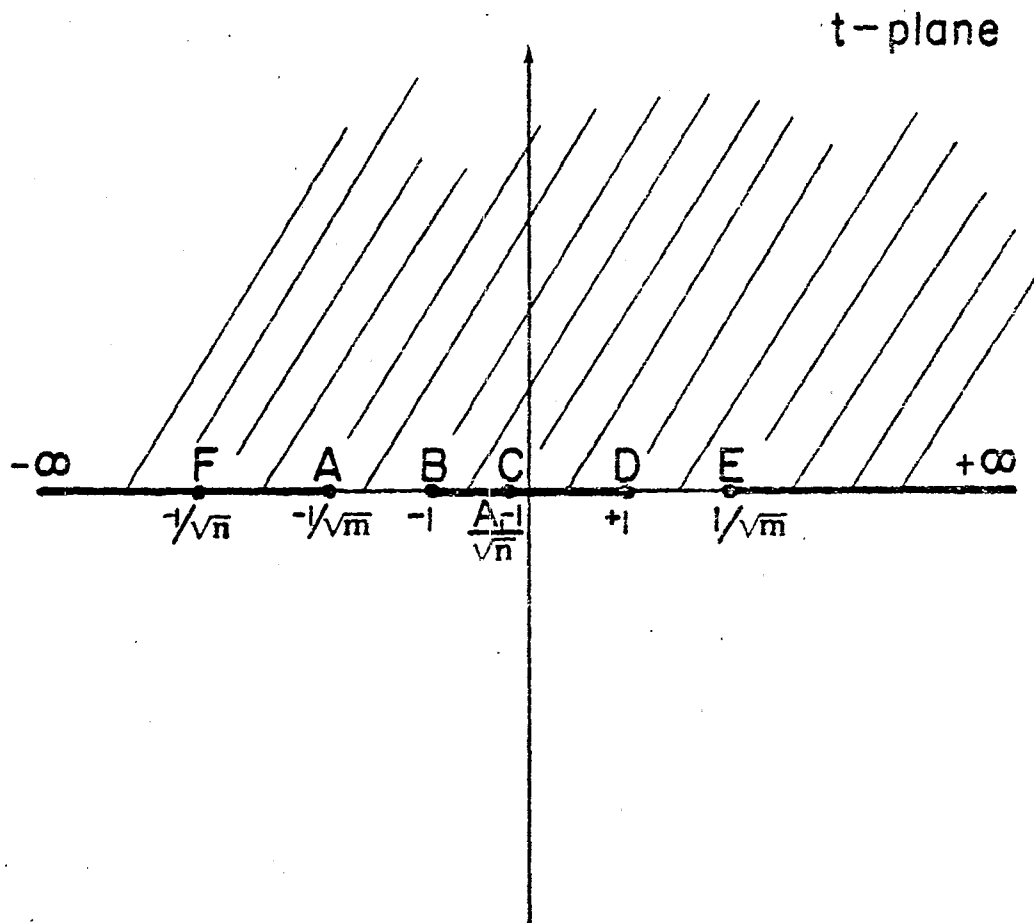


Figure 5. The shaded region of Figure 4 is conformally mapped onto the upper-half t-plane.

$$u = F(\varphi|m)$$

$$= \int_0^{\varphi} [(1-t'^2)(1-mt'^2)]^{-\frac{1}{2}} dt'$$

$$\Pi(n;u|m) = \Pi(n;\varphi|\alpha)$$

$$= \int_0^{\varphi} (1-nt'^2)^{-1} [(1-t'^2)(1-mt'^2)]^{-\frac{1}{2}} dt'$$

$$f(m,n,u) = \frac{1}{2\sqrt{(1-n)(m-n)}} \ln \left\{ \frac{2(1-n)(m-n) + (1-n \operatorname{sn}^2 u)(n+nm-2m)}{n(m-1)(1-n \operatorname{sn}^2 u)} \right. \\ \left. + \frac{2n\sqrt{(1-n)(m-n)} \operatorname{cn} u \operatorname{dn} u}{n(m-1)(1-n \operatorname{sn}^2 u)} \right\}$$

and $\operatorname{sn} u$, $\operatorname{cn} u$, $\operatorname{dn} u$ are elliptic functions, and u and Π are elliptic integrals of the first kind and of the third kind.

In the transformation equation (10) there are five constants A_1 , B_1 , C_1 , m and n . To determine them we require the mapping among the boundary points (see Figs. 4 and 5) as shown in Table I. Here, $K(m)$ is the complete elliptic

Table I. Mapping of boundary points.

z_1 -plane	t -plane	u -value
$i\pi$	$-1/\sqrt{m}$	$-K(m) + iK'(m)$
$i\theta_0$	-1	$-K(m)$
$i\theta_0 + \operatorname{sinh}^{-1}(a/b \sin \theta_0)$	$-(1-A_1)/\sqrt{n}$	$\operatorname{sn}^{-1}[(A_1-1)/\sqrt{n}]$
$i\theta_0$	1	$K(m)$
0	$1/\sqrt{m}$	$K(m) + iK'(m)$

integral of the first kind. The third column of Table I gives the values of u , where $u = F(\varphi|m)$, corresponding to the boundary points in the z_1 -plane and t -plane. From (10) and the above table we find

$$\begin{aligned} C_1 &= -\sqrt{(1-n)(m-n)}/(A_1\sqrt{n}) \\ B_1 &= i\theta_0 \end{aligned} \tag{11}$$

and m, n, A_1 satisfy the following three coupled equations:

$$K(m) - A_1 \Pi(n; K(m)|m) = 0$$

$$1 - 2\theta_0/\pi = F(\sin^{-1}\sqrt{n/m}|m)/K(m) \tag{12}$$

$$\sinh^{-1}(a/b \sin \theta_0) = \frac{\sqrt{(1-n)(m-n)}}{A_1\sqrt{n}} [F(\sin^{-1}\beta/m) - A_1 \Pi(n; \operatorname{sn}^{-1}\beta/m)] - G$$

where

$$G = \frac{1}{2} \ln \left[\frac{\sqrt{(1-n)(1-m\beta^2)} - \sqrt{(m-n)(1-\beta^2)}}{\sqrt{(1-n)(1-m\beta^2)} + \sqrt{(m-n)(1-\beta^2)}} \right]$$

$$\beta = (1-A_1)/\sqrt{n}$$

The solution for the geometry shown in Fig. 5 is known [4,5]. Instead of translating the known solution in terms of our notation, it is more expedient to solve the problem anew. The Schwarz-Christoffel transformation required to map the upper half t -plane (Fig. 5) to the interior of a rectangle (Fig. 6) is

$$\begin{aligned} W = U + iV &= C_3 \int_0^t \frac{dt'}{\sqrt{(1-t'^2)(1-mt'^2)}} + B_3 \\ &= C_3 u + B_3 \end{aligned} \tag{13}$$

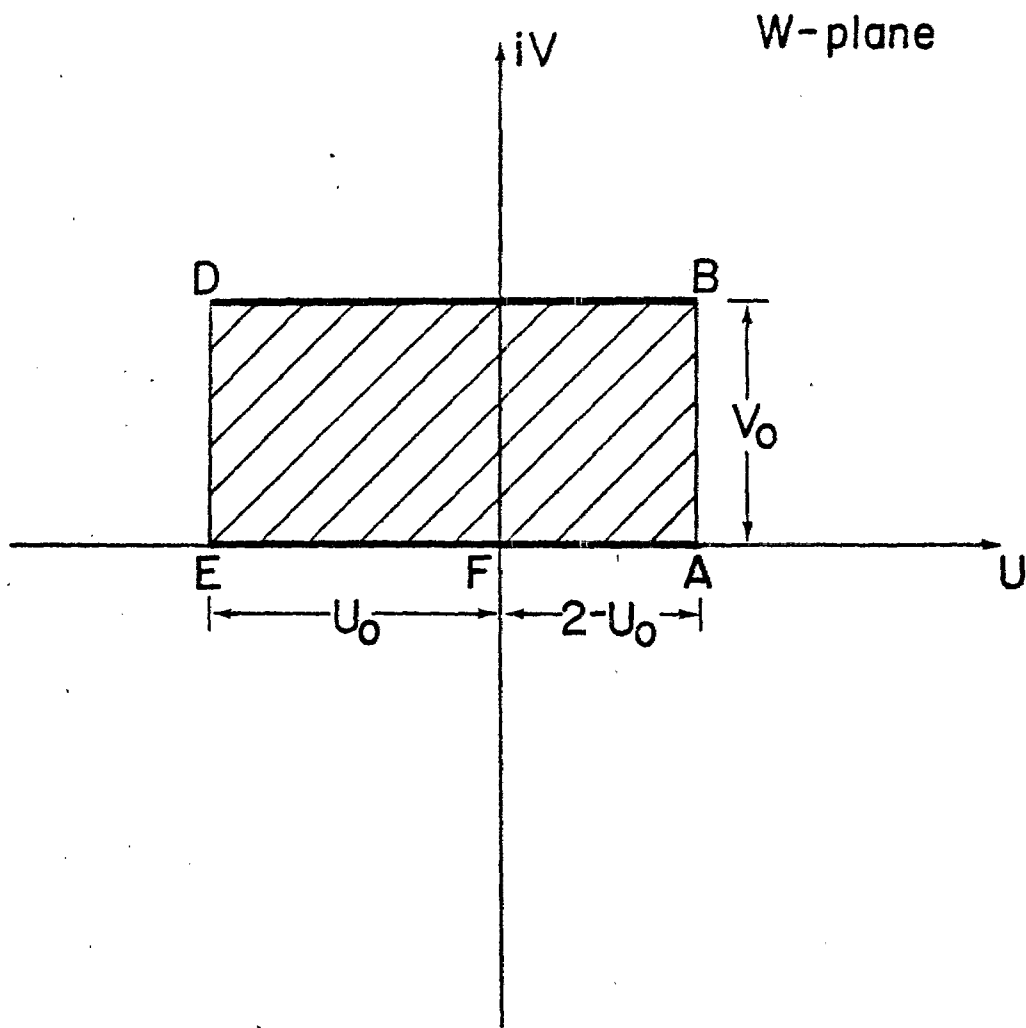


Figure 6. The entire upper-half t -plane (Figure 5) is conformally mapped onto a rectangle in the W -plane.

Table II shows the mapping among the boundary points. From (13) and Table II

Table II. Mapping of boundary points.

t-plane	W-plane	u-value
$-1/\sqrt{m}$	$2 - U_0$	$-K(m) + iK'(m)$
-1	$2 - U_0 + iV_0$	$-K(m)$
1	$-U_0 + iV_0$	$K(m)$
$1/\sqrt{m}$	$-U_0$	$K(m) + iK'(m)$
$-1/\sqrt{n}$	0	$\text{sn}^{-1}(-1/\sqrt{n})$

we find

$$C_3 = -1/K(m)$$

$$V_0 = K'(m)/K(m)$$

$$U_0 = 1 + F(\sin^{-1}\sqrt{n/m}|m)/K(m)$$

$$B_3 = iK'(m)/K(m) - F(\sin^{-1}\sqrt{n/m}|m)/K(m)$$

Thus, (13) gives

$$u = -WK(m) + iK'(m) - F(\sin^{-1}\sqrt{n/m}|m) \quad (14)$$

The geometric impedance factor f_g is given by

$$f_g = \frac{\Delta V}{\Delta U}$$

where ΔV is the normalized potential difference between two plates and ΔU is the change in the normalized stream function on one plate. For the rectangular geometry shown in Fig. 6 we have $\Delta V = V_0 = K'(m)/K(m)$ and $\Delta U = 2$. Hence,

$$f_g = \frac{1}{2} \frac{K'(m)}{K(m)} \quad (15)$$

It is easy to convince oneself that expression (15) is also the geometric impedance factor for the original two conical plates. The characteristic impedance can be obtained simply from

$$\begin{aligned} Z_c &= \sqrt{\mu/\epsilon} f_g \\ &= \frac{1}{2} \sqrt{\frac{\mu}{\epsilon}} \frac{K'(m)}{K(m)} \end{aligned} \quad (16)$$

where m is determined by (12).

For the special case where $\theta_0 = \pi/2$, one can solve (12) analytically and get

$$\begin{aligned} n &= 0 \\ A_1 &= 1 \\ m &= a^2/(a^2+b^2) \end{aligned} \quad (17)$$

from which, together with (16), one can show that the same Z_c value results as that reported earlier in [6,7].

Before proceeding to the numerical tabulation and graphical presentation of f_g and Z_c let us point out that in the limit of small cone angles, the parameter m used in this note will not reduce to the parameter m used in previous reports, such as [8] and [9]. If one insists on using an m which reduces to the previous m in the limiting case, one has to relabel the boundary points of Fig. 5. This means that all the subsequent transformations will be different. Instead of

reworking the problem we suggest in Fig. 7 the necessary mapping that goes from Fig. 4 to Fig. 5. This mapping is expected to give $f_g = K'(m)/K(m)$, in which the parameter m would reduce in the limiting case to the one previously used.

Fig. 8 is a plot of the geometric impedance factor f_g versus l/b with b/a as a parameter, whereas Fig. 9 displays f_g versus b/a with l/b as a parameter. It is interesting to note that the two limiting curves (indicated by $l/b = 0$ and $l/b = \infty$) of Fig. 9 give a very good bound for all b/a values. The limiting curve ($l/b = 0$) has been reported in [6] and the other limiting curve ($l/b = \infty$) corresponds to the two-parallel-plate case.

In Table III are tabulated the m values resulting from numerically solving (12). From these m values f_g and Z_c are calculated according to (15) and (16) and tabulated respectively in Tables IV and V.

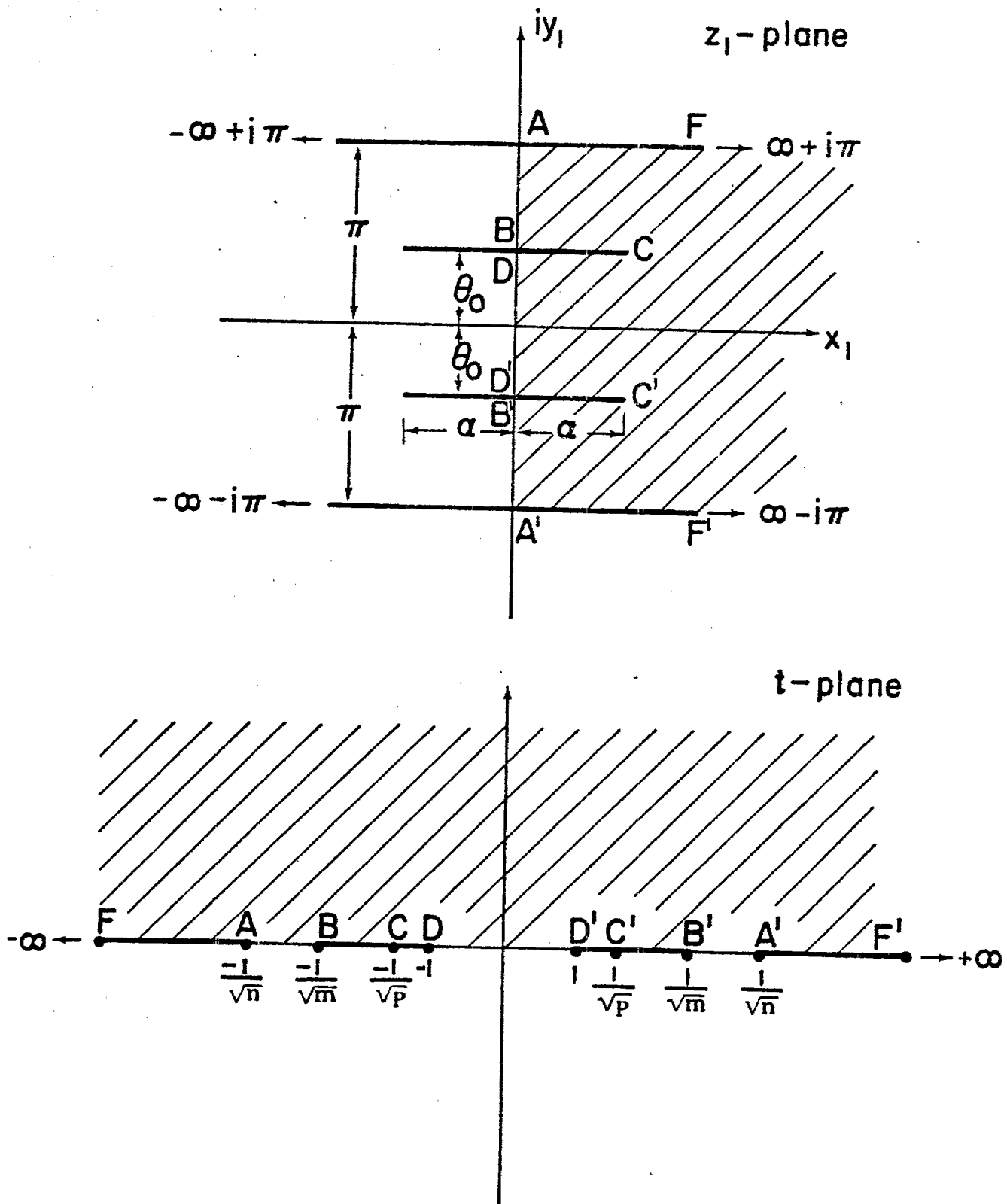


Figure 7. A suggested conformal mapping in which the parameter m would reduce to that often used for two parallel plates.

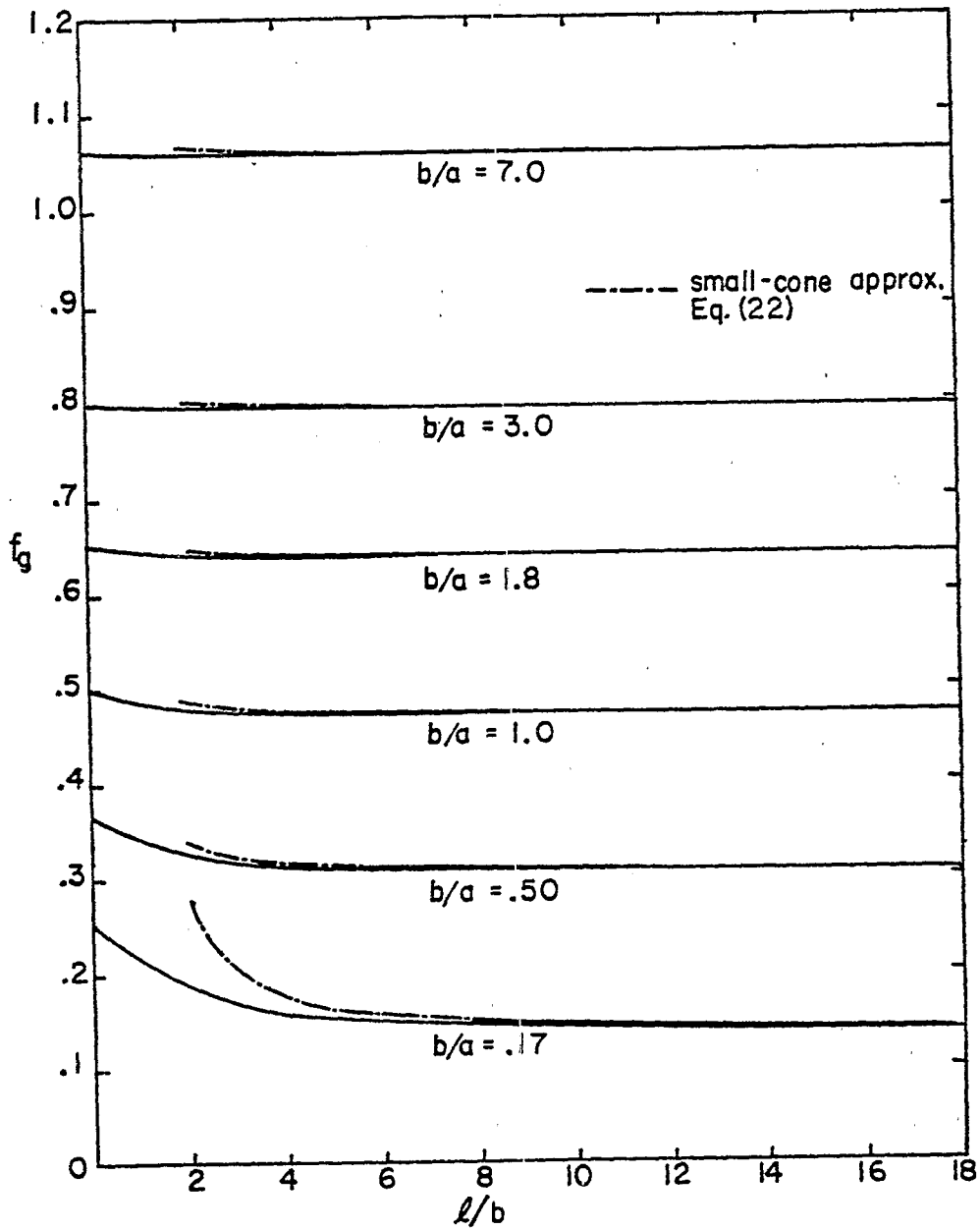


Figure 8. Geometric impedance factor f_g of two conical plates versus l/b .

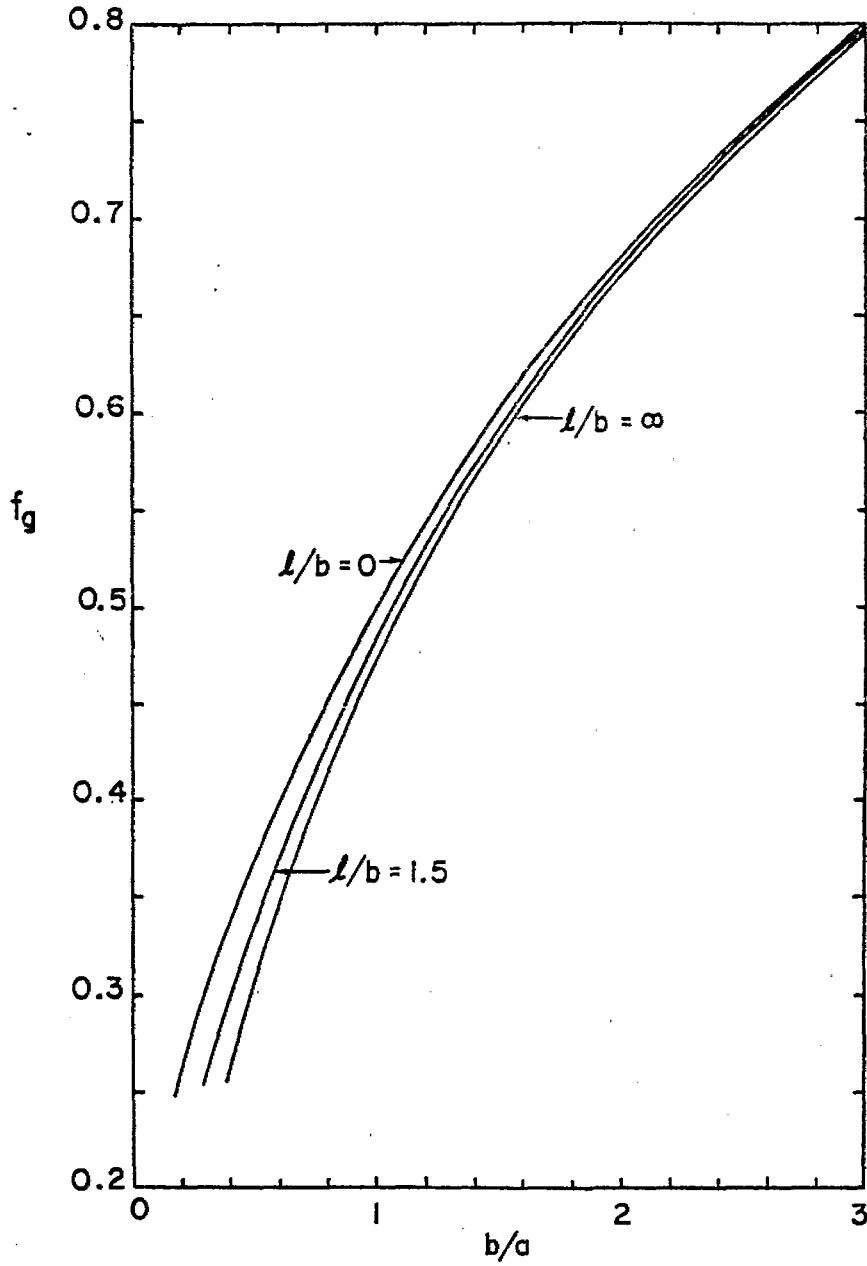


Figure 9. Geometric impedance factor f_g of two conical plates versus b/a .

ℓ/b b/a	0.00	1.00	1.50	2.00	2.50	3.00	3.50	3.90	4.50	5.00	10.0
.17	.9720	.9880	.9936	.9964	.9978	.9985	.9989	.9992	.9994	.9995	.9998
.41	.8561	.8974	.9170	.9294	.9371	.9421	.9455	.9474	.9495	.9508	.9551
.50	.8000	.8439	.8653	.8789	.8875	.8931	.8969	.8991	.9014	.9028	.9076
.60	.7353	.7785	.7996	.8130	.8215	.8270	.8306	.8328	.8350	.8364	.8411
.70	.6711	.7112	.7305	.7428	.7504	.7554	.7586	.7605	.7626	.7638	.7679
.80	.6098	.6454	.6624	.6730	.6796	.6838	.6866	.6882	.6899	.6910	.6944
.90	.5525	.5834	.5979	.6069	.6124	.6159	.6182	.6195	.6209	.6218	.6246
1.00	.5000	.5264	.5386	.5460	.5505	.5534	.5553	.5564	.5575	.5582	.5605
1.20	.4098	.4286	.4369	.4419	.4450	.4469	.4481	.4488	.4496	.4500	.4515
1.24	.3941	.4115	.4193	.4239	.4267	.4284	.4296	.4302	.4309	.4313	.4327
1.40	.3378	.3510	.3567	.3601	.3621	.3634	.3642	.3647	.3652	.3655	.3665
1.60	.2809	.2902	.2941	.2965	.2978	.2987	.2992	.2996	.2999	.3001	.3008
1.80	.2359	.2425	.2453	.2469	.2478	.2484	.2488	.2490	.2493	.2494	.2499
2.00	.2000	.2048	.2068	.2080	.2086	.2091	.2093	.2095	.2096	.2097	.2101
2.50	.1379	.1403	.1412	.1417	.1421	.1422	.1424	.1424	.1425	.1426	.1427
3.00	.1000	.1012	.1017	.1020	.1022	.1023	.1023	.1024	.1024	.1024	.1025
7.00	.0200	.0201	.0201	.0201	.0201	.0201	.0201	.0201	.0201	.0201	.0201

Table III. Values of the parameter m .

$\frac{a}{b}$ \ / $\frac{b}{a}$	0.00*	1.00	1.50	2.00	2.50	3.00	3.50	3.90	4.50	5.00	10.0	∞ **
.17	.2481	.2186	.2008	.1871	.1769	.1692	.1633	.1595	.1551	.1522	.1403	.1351
.41	.3389	.3144	.3010	.2916	.2853	.2809	.2778	.2760	.2740	.2727	.2684	.2667
.50	.3676	.3455	.3338	.3259	.3207	.3172	.3148	.3133	.3118	.3109	.3076	.3064
.60	.3974	.3778	.3678	.3613	.3571	.3543	.3524	.3513	.3502	.3494	.3470	.3461
.70	.4254	.4080	.3995	.3941	.3907	.3884	.3870	.3861	.3852	.3846	.3827	.3820
.80	.4517	.4364	.4291	.4246	.4217	.4199	.4187	.4180	.4173	.4168	.4153	.4148
.90	.4765	.4630	.4568	.4529	.4506	.4491	.4481	.4475	.4469	.4465	.4453	.4449
1.00	.5000	.4881	.4827	.4794	.4774	.4761	.4753	.4748	.4743	.4740	.4730	.4726
1.20	.5433	.5339	.5298	.5274	.5259	.5250	.5244	.5240	.5237	.5234	.5227	.5225
1.24	.5515	.5425	.5386	.5362	.5349	.5340	.5334	.5331	.5328	.5326	.5319	.5317
1.40	.5825	.5749	.5717	.5698	.5687	.5680	.5675	.5673	.5670	.5668	.5663	.5661
1.60	.6179	.6118	.6092	.6077	.6068	.6063	.6059	.6057	.6055	.6054	.6050	.6048
1.80	.6503	.6452	.6432	.6419	.6412	.6408	.6405	.6404	.6402	.6401	.6397	.6396
2.00	.6800	.6758	.6741	.6731	.6725	.6721	.6719	.6718	.6716	.6715	.6713	.6712
2.50	.7449	.7420	.7409	.7402	.7399	.7396	.7395	.7394	.7393	.7393	.7391	.7390
3.00	.7994	.7974	.7966	.7961	.7958	.7957	.7956	.7955	.7955	.7954	.7953	.7953
7.00	1.0623	1.0619	1.0617	1.0616	1.0616	1.0616	1.0615	1.0615	1.0615	1.0615	1.0615	1.0615

* Two planar conical plates

** Two parallel plates

Table IV. Values of the g_{ic} impedance factor f_g.

λ/b b/a	0.0*	1.00	1.50	2.00	2.50	3.00	3.50	3.90	4.50	5.00	10.0	∞ **
.17	93.47	82.35	75.66	70.50	66.64	63.73	61.51	60.10	58.43	57.34	52.86	50.90
.41	127.7	118.5	113.4	109.9	107.5	105.8	104.7	104.0	103.2	102.8	101.1	100.4
.50	138.5	130.2	125.8	122.8	120.8	119.5	118.6	118.1	117.5	117.1	115.9	115.4
.60	149.7	142.3	138.6	136.1	134.5	133.5	132.8	132.4	131.9	131.7	130.7	130.4
.70	160.3	153.7	150.5	148.5	147.2	146.3	145.8	145.5	145.1	144.9	144.2	143.9
.80	170.2	164.4	161.7	159.9	158.9	158.2	157.7	157.5	157.2	157.0	156.5	156.3
.90	179.5	174.4	172.1	170.6	169.7	169.2	168.8	168.6	168.4	168.2	167.8	167.6
1.00	188.4	183.9	181.8	180.6	179.8	179.4	179.1	178.9	178.7	178.6	178.2	178.0
1.20	204.7	201.1	199.6	198.7	198.1	197.8	197.5	197.4	197.3	197.2	196.9	196.8
1.24	207.8	204.4	202.9	202.0	201.5	201.2	201.0	200.8	200.7	200.6	200.4	200.3
1.40	219.4	216.6	215.4	214.7	214.2	214.0	213.8	213.7	213.6	213.5	213.3	213.3
1.60	232.8	230.5	229.5	229.0	228.6	228.4	228.3	228.2	228.1	228.1	227.9	227.9
1.80	245.0	243.1	242.3	241.8	241.6	241.4	241.3	241.2	241.2	241.1	241.0	241.0
2.00	256.2	254.6	253.9	253.6	253.3	253.2	253.1	253.1	253.0	253.0	252.9	252.9
2.50	280.6	279.6	279.1	278.9	278.7	278.6	278.6	278.6	278.5	278.5	278.4	278.4
3.00	301.2	300.4	300.1	299.9	299.8	299.8	299.7	299.7	299.7	299.7	299.6	299.6
7.00	400.2	400.0	400.0	400.0	399.9	399.9	399.9	399.9	399.9	399.9	399.9	399.9

* Two planar conical plates

** Two parallel plates

Table V. Values of the characteristic impedance Z_c of two conical plates.

IV. SMALL CONE ANGLES

When θ_0 is exactly zero, (12) is simplified to

$$\begin{aligned} n &= m \\ A_1 &= (1-m)K(m)/E(m) \\ \frac{a}{b} \frac{\pi}{2} &= K(m)Z(\operatorname{sn}^{-1}q|m) + q\sqrt{m} K(m) \end{aligned} \quad (18)$$

where

$$q^2 = [m - (1-A_1)^2] / [m - m(1-A_1)^2]$$

and $E(m)$ is the complete elliptic integral of the second kind and $Z(u|m)$ is the Jacobi's Zeta function [3]. The solution of (18) together with (15) will give the same geometric impedance factor as that of the parallel plates. The truth of this statement will be shown below for the two extreme cases where $a/b \ll 1$ and $a/b \gg 1$.

For $a/b \ll 1$, (18) gives

$$m \approx (a/b)^2$$

and from (15) we get

$$f_g \approx \frac{1}{\pi} \ln(4b/a) \quad (19.a)$$

For $a/b \gg 1$, (18) gives

$$1-m \approx 16\sqrt{b/(\pi a)} e^{-[1+a\pi/(2b)]}$$

and from (15) we get

$$f_g \approx \frac{b}{a} \left[1 + \frac{b}{\pi a} \left(2 + \ln \frac{a\pi}{b} \right) \right]^{-1} \quad (19.b)$$

The results (19.a) and (19.b) agree with those given in [9].

If one wants to look into the effects of small cone angles for which $1 \gg \theta_0 > 0$, (12) is too complicated to be solved analytically. An alternative approach will now be given. In the z_1 -plane shown in Fig. 4, the charge distribution $\sigma(x_1)$ on the upper plate can be obtained by solving the integral equation

$$V_0 = -\frac{1}{\epsilon} \int_{-\alpha}^{\alpha} G(\theta_0, \theta_0; x_1, x'_1) \sigma(x'_1) dx'_1$$

where $\alpha = \sinh^{-1}(a/b \sin \theta_0)$, V_0 is the potential on the upper plate located at $y_1 = \theta_0$, and $G(y_1, y'_1; x_1, x'_1)$ is the Green's function that satisfies

$$\nabla^2 G(y_1, y'_1; x_1, x'_1) = -\delta(y_1 - y'_1) \delta(x_1 - x'_1)$$

$$G(\pm\pi, y'_1; x_1, x'_1) = 0$$

Then f_g is obtained from

$$f_g = \frac{-\int_{-\alpha}^{\alpha} G(\theta_0, \theta_0; x_1, x'_1) \sigma(x'_1) dx'_1}{\int_{-\alpha}^{\alpha} \sigma(x'_1) dx'_1} \quad (20)$$

In the small-cone-angle case, the two central plates of Fig. 4 become very narrow and close to each other, and the conditions $\theta_0 \ll \pi$ and $\sinh^{-1}(a/b \sin \theta_0) \ll 1$ generally hold. With these conditions in mind one obtains, after some straightforward manipulation,

$$G(\theta_0, \theta_0; x_1, x'_1) \approx \frac{1}{4\pi} \ln \left(\frac{(x_1 - x'_1)^2}{4\theta_0^2 + (x_1 - x'_1)^2} \right) + \frac{\theta_0^2}{12\pi}$$

Then with the aid of (20) one has

$$f_g = \bar{f}_g(\theta_0/\alpha) - \theta_0^2/12\pi \quad (21)$$

where $\bar{f}_g(\theta_0/\alpha)$ is the geometric impedance factor for two parallel plates with separation $2\theta_0$ and width $2\alpha = 2 \sinh^{-1}(a/b \sin \theta_0)$.

Under the condition $a/b \sin \theta_0 \ll 1$, (21) can be further approximated by

$$\begin{aligned} f_g &= \bar{f}_g(b/a + [b/a + a/b]\theta_0^2/6) - \theta_0^2/12\pi \\ &= \bar{f}_g(b/a) + \delta_{cp} \theta_0^2 \end{aligned} \quad (22)$$

with

$$6\delta_{cp} = (b/a + a/b)\bar{f}'_g(b/a) - 1/(2\pi)$$

where \bar{f}'_g is the derivative of \bar{f}_g with respect to the argument. For the b/a values of interest, $\bar{f}_g(b/a)$ can be found in [8] and, after some manipulation, $\bar{f}'_g(b/a)$ can be calculated by using the "m" values obtained in [8]. The values of \bar{f}_g and δ_{cp} are listed in Table VI and plotted in Fig. 10. The approximate equation (22) for small cone angles has been plotted in Fig. 8.

Table VI: Values of \bar{f}_g and δ_{cp}

b/a	$\bar{f}_g(b/a)$	δ_{cp}
0.17	0.1334	0.6609
0.41	0.2654	0.1963
0.5	0.3064	0.1479
0.6	0.3461	0.1159
0.7	0.3820	0.0950
0.8	0.4148	0.0806
0.9	0.4449	0.0702
1.0	0.4726	0.0626
1.2	0.5225	0.0522
1.24	0.5306	0.0508
1.4	0.5661	0.0457
1.6	0.6048	0.0414
1.8	0.6396	0.0384
2.0	0.6712	0.0362
2.5	0.7390	0.0328
3.0	0.7953	0.0309
7.0	1.0610	0.0273

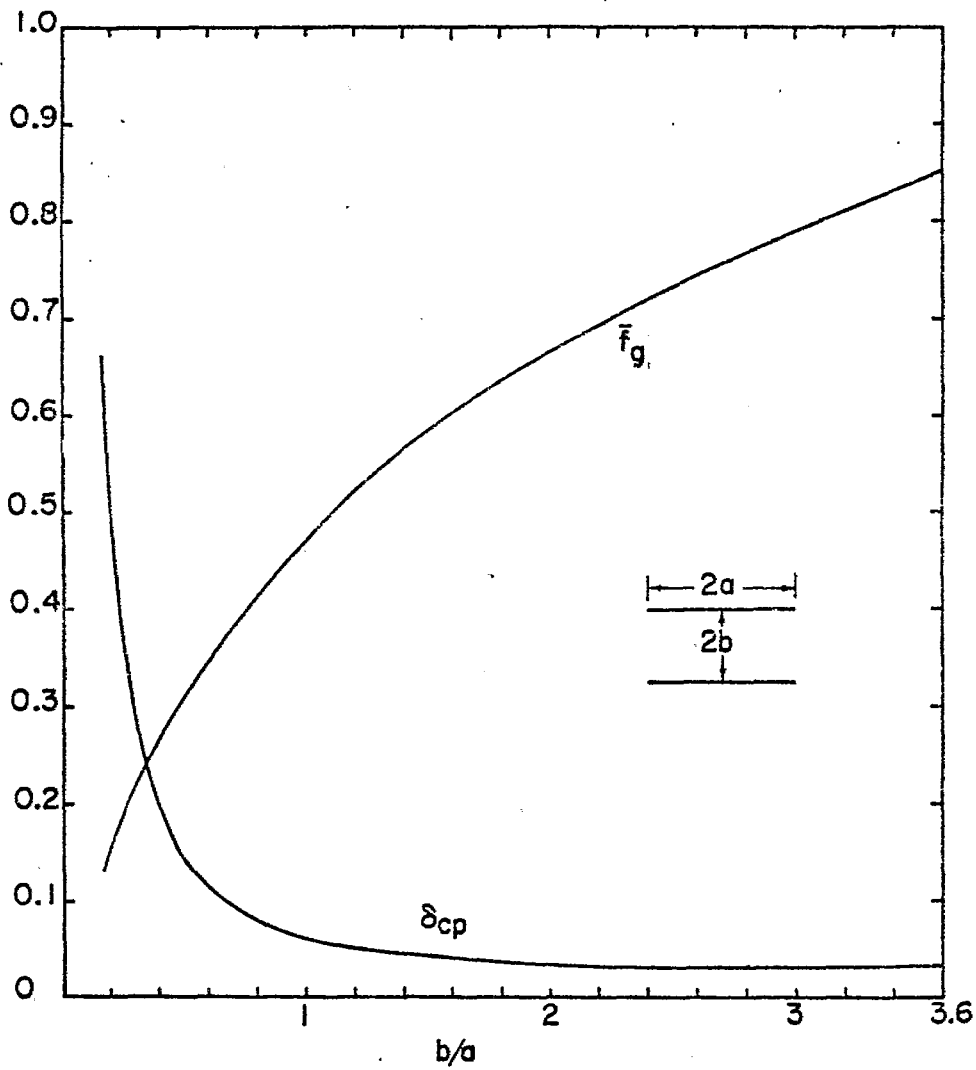


Figure 10. Geometric impedance factor \bar{f}_g of two parallel plates and the small-cone-angle correction coefficient δ_{cp} .

$$f_g = \bar{f}_g + \delta_{cp} (b/l)^2$$

ACKNOWLEDGMENT

The authors had helpful discussions with L. Marin of Dikewood, C.E. Baum, K.C. Chen and D.V. Giri of Air Force Weapons Laboratory during the course of the work. J.P. Martinez of Dikewood has helped in the numerical work.

REFERENCES

- [1] C.E. Baum, "Early time performance at large distances of periodic planar arrays of planar bicones with sources triggered in a plane-wave sequence," *Sensor and Simulation Note* 184, August 1973.
- [2] W.R. Smythe, Static and Dynamic Electricity, 2nd ed., McGraw-Hill, 1950, § 6.20.
- [3] M. Abramowitz and I.A. Stegun, Handbook of Mathematical Functions, National Bureau of Standards, Applied Mathematics Series 55, 1970, Chapters 16 and 17.
- [4] A.E.H. Love, "Some electrostatic distribution in two dimensions," *Proc. London Math. Soc.* Vol. 22, 1924, p.337.
- [5] P. Moon and D.E. Spencer, Field Theory Handbook, Springer-Verlag, 1961, p.71, p.54.
- [6] C.E. Baum, "A conical-transmission-line gap for a cylindrical loop," *Sensor and Simulation Note* 42, May 1967.
- [7] T.K. Liu, "Impedances and field distributions of curved parallel-plate transmission-line simulators," *Sensor and Simulation Note* 170, Feb. 1973.
- [8] C.E. Baum, D.V. Giri, R.D. Gonzalez, "Electromagnetic field distribution of the TEM mode in a symmetrical two-parallel-plate transmission line," *Sensor and Simulation Note* 219, April 1976.
- [9] C.E. Baum, "Impedance and field distributions for parallel plate transmission line simulators," *Sensor and Simulation Note* 21, June 1966.